

1 **A CONTINUATION MULTIPLE SHOOTING METHOD FOR**
 2 **WASSERSTEIN GEODESIC EQUATION***

3 JIANBO CUI^{††}, LUCA DIECI[†], AND HAOMIN ZHOU[†]

4 **Abstract.** In this paper, we propose a numerical method to solve the classic L^2 -optimal trans-
 5 port problem. Our algorithm is based on use of multiple shooting, in combination with a continuation
 6 procedure, to solve the boundary value problem associated to the transport problem. We exploit
 7 the viewpoint of Wasserstein Hamiltonian flow with initial and target densities, and our method is
 8 designed to retain the underlying Hamiltonian structure. Several numerical examples are presented
 9 to illustrate the performance of the method.

10 **Key words.** Hamiltonian flow; boundary value problem; optimal transport; multiple-shooting
 11 method

12 **AMS subject classifications.** 49Q22, 49M25, 65L09, 34A55

13 **1. Introduction.** Optimal transport (OT) has a long and rich history, and it
 14 finds applications in various fields, such as image processing, machine learning and
 15 economics (e.g., see [19, 25]). The first mass transfer problem, a civil engineering
 16 problem, was considered by Monge in 1781. A modern treatment of this problem,
 17 in term of probability densities, was studied by Kantorovich in [16]. In this light,
 18 the optimal transport problem consists in moving a certain probability density into
 19 another, while minimizing a given cost functional. Depending on whether (one or
 20 both of) the densities are continuous or discrete, one has a fully discrete, or a semi-
 21 discrete, or a continuous OT problem. In this work, we consider a continuous OT
 22 problem subject to the cost given by the squared L^2 norm. This is the most widely
 23 studied continuous OT problem, and the formulation we adopt in this paper is based
 24 on an optimal control formulation in a fluid mechanics framework, known as *Benamou-
 25 Brenier formula*, established in [3]. The starting point is to cast the OT problem in
 26 a variational form as

27 (1.1)
$$\inf_v \left\{ \int_0^1 \langle v, v \rangle_\rho dt : \partial_t \rho + \nabla \cdot (\rho v) = 0, \rho(0) = \mu, \rho(1) = \nu \right\},$$

28 where $\langle v, v \rangle_\rho := \int_{\mathbb{R}^d} |v|^2 \rho dx$ with smooth velocity field $v(t, x) \in \mathbb{R}^d$, and μ and ν are
 29 probability density functions satisfying $\int_{\mathbb{R}^d} |x|^2 \mu(x) dx, \int_{\mathbb{R}^d} |x|^2 \nu(x) dx < +\infty$. This
 30 ensures the existence and uniqueness of the optimal map M^* for the equivalent Monge-
 31 Kantorovich problem of (1.1), i.e., $\inf_M \int_{\mathbb{R}^d} |M(x) - x|^p \mu(x) dx$ with $M : \mathbb{R}^d \rightarrow \mathbb{R}^d$
 32 transferring μ to ν (see e.g., [25, Theorem 1.22]). Moreover, the optimal map has the
 33 form $M^*(x) = \nabla \psi(x) = x + \nabla \phi(x)$, μ -a.s., with a convex function $\psi(x)$. From [3],
 34 we have that $\nabla \phi(x) = v(0, x)$ and that the characteristic line $(X(t, x), v(t, X(t, x)))$
 35 satisfies

36
$$\partial_t \rho(t, X(t, x)) + \nabla \cdot (\rho(t, X(t, x)) v(t, X(t, x))) = 0,$$

37
$$\partial_t v(t, X(t, x)) + \nabla \left(\frac{1}{2} |v(t, X(t, x))|^2 \right) = 0.$$

38 *The research is partially support by Georgia Tech Mathematics Application Portal (GT-MAP)
 and by research grants NSF DMS-1620345, DMS-1830225, and ONR N00014-18-1-2852.

†School of Mathematics, Georgia Institute of Technology, Atlanta, GA 30332, USA.
 (jcui82@math.gatech.edu, luca.dieci@math.gatech.edu, hmzhou@math.gatech.edu)

39 When $X(t, x) = x + tv(0, x)$ is invertible, we obtain that $\rho(t) = X(t, \cdot)^\# \rho(0)$ and that
 40 $v(t, x) = v(0, X^{-1}(t, x)) = \nabla \psi(0, X^{-1}(t, x))$. We refer to [5, 13, 25] and references
 41 therein for results about regularity of M^* and ψ . The optimal value in (1.1) is known
 42 as the L^2 -Wasserstein distance square between μ and ν , and written as $g_W^2(\mu, \nu)$. The
 43 formulation (1.1) is interpreted as finding the optimal vector field v to transport the
 44 given density function μ to the density ν with the minimal amount of kinetic energy.
 45 (We emphasize that the “time variable” t has no true physical meaning, and it serves
 46 the role of a homotopy parameter.)

47 By introducing the new variable S satisfying $v = \nabla S$, the critical point of (1.1)
 48 satisfies (up to a spatially independent function $C(t)$) the following system in the
 49 unknowns (ρ, S) :

50 (1.2)
$$\begin{cases} \partial_t \rho + \nabla \cdot (\rho \nabla S) = 0 \\ \partial_t S + \frac{1}{2} |\nabla S|^2 = 0, \end{cases}$$

51 subject to boundary conditions $\rho(0) = \mu, \rho(1) = \nu$. This is the well-known geodesic
 52 equation between two densities μ and ν on the Wasserstein manifold [27], and can
 53 also be viewed as a Wasserstein Hamiltonian flow with the Hamiltonian $H(\rho, S) =$
 54 $\frac{1}{2} \int_{\mathbb{R}^d} |\nabla S|^2 \rho dx$ when $C(t) = 0$, [8]. If $S^0 = S|_{t=0}$ is known, the optimal value
 55 $g_W(\mu, \nu)$, the L^2 -Wasserstein distance between μ and ν , equals $\sqrt{2H(\mu, S^0)}$.

56 *REMARK 1.1.* *Obviously, S is defined only up to an arbitrary constant. As a consequence, the (ρ, S) formulation (1.2) of the boundary value problem cannot have a unique solution. Because of this fact, we will in the end reverse to using a formulation based on ρ and v , but the Hamiltonian structure of (1.2) will guide us in the development of appropriate semi-discretizations of the problem in the (ρ, v) variables.*

61 In recent years, there have been several numerical studies concerned with approximating solutions of OT problems, and many of them are focused on the continuous problem considered in this work, that is on computation of the Wasserstein distance g_W and the underlying OT map. A key result in this context is that the optimal map is the gradient of a convex function u , which is the solution of the so-called Monge-Ampère equation, a non linear elliptic PDE subject to non-standard boundary conditions. We refer to [2, 4, 12, 15, 21, 23, 28], for a sample of numerical work on the solution of the Monge-Ampère equation. For different approaches, in the case of continuous, discrete, and semi-discrete OT problems, and for a variety of cost functions, we refer to [6, 10, 11, 18, 20, 22, 24, 26].

71 However, numerical approximation of the solution of the geodesic equation has
 72 received little attention, and this is our main scope in this computational paper. There
 73 are good reasons to consider solving the geodesic equation: at once one can recover the
 74 Wasserstein distance, the OT map, and the “time dependent” vector field producing
 75 the optimal trajectory. At the same time, there are also a number of obstacles that
 76 make the numerical solution of the Wasserstein geodesic equation very challenging:
 77 the density ρ needs to be non-negative, mass conservation is required, and retaining
 78 the underlying symplectic structure is highly desirable too. Another hurdle, which
 79 is not at all obvious, is that the Hamiltonian system (1.2) with initial values on the
 80 Wasserstein manifold often develops singularities in finite time (see e.g. [9]). These
 81 challenges must be overcome when designing numerical schemes for the boundary
 82 value problem (1.2).

83 In this paper, we propose to compute the solution of (1.2) by combining a multiple
 84 shooting method, in conjunction with a continuation strategy, for an appropriate semi-

85 discretization of (1.2). First, we consider a spatially discretized version of (1.2), which
 86 will give a (large) boundary value problem of ODEs. To solve the latter, we will use
 87 a multiple shooting method, whereby the interval $[0, 1]$ is partitioned into several
 88 subintervals, $[0, 1] = \bigcup_{i=0}^{K-1} [t_i, t_{i+1}]$, initial guesses for the density and the velocity are
 89 provided at each t_i , $i = 0, \dots, K - 1$, initial value problems are solved on $[t_i, t_{i+1}]$,
 90 and eventually enforcement of continuity and boundary conditions will result in a
 91 large nonlinear system to solve for the density ρ and velocity v at each t_i . To solve
 92 the nonlinear system, we use Newton's method, and –to enhance its convergence
 93 properties– we will adopt a continuation method to obtain good initial guesses for the
 94 Newton's iteration.

95 Multiple shooting is a well studied technique for solving two-point boundary value
 96 problems of ordinary differential equations (TPBVPs of ODEs), and we refer to [17] for
 97 an early derivation of the method, and to [1] for a comprehensive review of techniques
 98 for solving TPBVPs of ODEs, and relations (equivalence) between many of them.
 99 Our main reason for adopting multiple shooting is its overall simplicity, and the
 100 ease with which we can adopt appropriate time discretizations of symplectic type (on
 101 sufficiently short time intervals) in order to avoid finite time singularities when solving
 102 (1.2) subject to given initial conditions.

103 The rest of paper is organized as follows. In Section 2, we briefly review the
 104 continuous OT problem and introduce a spatial discretization to convert (1.2) into
 105 Hamiltonian ODEs. At first, we propose the semi-discretization for the (ρ, S) vari-
 106 ables, but then in Section 3 we will revert it to the (ρ, v) variables, which are those
 107 with which we end up working. The multiple shooting method, and the continua-
 108 tion strategy, are also presented in Section 3. Results of numerical experiments are
 109 presented in Section 4.

110 **2. Spatially discrete OT problems.** In this section, we introduce the spatial
 111 discretization of (1.2). First of all, we need to truncate \mathbb{R}^d to a finite computational
 112 domain, which for us will be a d -dimensional rectangular box in \mathbb{R}^d : $\mathcal{O} = [x_L, x_R]^d$.
 113 We note that truncating \mathbb{R}^d to a domain like \mathcal{O} is effectively placing some natural
 114 condition on the type of densities μ and ν we envision having, namely they need to
 115 decay sufficiently fast outside of the box \mathcal{O} ([14]). Then, we propose the spatial dis-
 116cretization of (1.2), by following the theory of OT problem on a finite graph similarly
 117 to what we did in [9].

118 Next, we let $G = (V, E)$ be a uniform lattice graph with equal spatial step-size
 119 $\delta x = \frac{x_R - x_L}{n}$ in each dimension. Here V is the vertex set with $N = (n + 1)^d$ nodes
 120 labeled by multi-index $i = (i_k)_{k=1}^d \in V, i_k \leq n + 1$. E is the edge set: $ij \in E$ if
 121 $j \in N(i)$ (read, j is a neighbor of i), where

$$122 \quad 123 \quad N(i) = \bigcup_{k=1}^d N_k(i), \quad N_k(i) = \left\{ (i_1, \dots, i_{k-1}, j_k, i_{k+1}, \dots, i_d) \mid |i_k - j_k| = 1 \right\}.$$

A vector field v on E is a skew-symmetric matrix. The inner product of two vector
 fields u, v is defined by

$$\langle u, v \rangle_{\theta(\rho)} := \frac{1}{2} \sum_{(j,l) \in E} u_{jl} v_{jl} \theta_{jl}(\rho),$$

124 where θ is a weight function depending on the probability density. In this study, we
 125 select it as the average of density on neighboring points, i.e.,

$$126 \quad (2.1) \quad \theta_{ij}(\rho) := \frac{\rho_i + \rho_j}{2}, \quad \text{if } j \in N(i).$$

127 For more choices, we refer to [9] and references therein.

The discrete divergence of the flux function ρv is defined as

$$\text{div}_G^\theta(\rho v) := -\left(\sum_{l \in N(j)} \frac{1}{\delta x^2} v_{jl} \theta_{jl}\right).$$

128 Using the discrete divergence and inner product, a discrete version of the Benamou-
129 Brenier formula is introduced in [7],

$$130 \quad W^2(\mu, \nu) = \inf_v \left\{ \int_0^1 \langle v, v \rangle_{\theta(\rho)} dt : \frac{d\rho}{dt} + \text{div}_G^\theta(\rho v) = 0, \rho(0) = \mu, \rho(1) = \nu \right\}. \\ 131$$

132 By the Hodge decomposition on graph, it is proved that the optimal vector field v can
133 be expressed as the gradient of potential function S defined on the node set V , i.e.
134 $v = \nabla_G S := (S_j - S_l)_{(j,l) \in E}$, ρ_t -a.s. Similarly, its critical point satisfies the discrete
135 Wasserstein Hamiltonian flow (cfr. with (1.2))

$$136 \quad (2.2) \quad \begin{aligned} \frac{d\rho_i}{dt} &= \sum_{j \in N(i)} \frac{1}{(\delta x)^2} (S_i - S_j) \theta_{ij}(\rho) = \frac{\partial \mathcal{H}}{\partial S_i}, \\ \frac{dS_i}{dt} &= -\frac{1}{2} \sum_{j \in N(i)} \frac{1}{(\delta x)^2} (S_i - S_j)^2 \frac{\partial \theta_{ij}(\rho)}{\partial \rho_i} = -\frac{\partial \mathcal{H}}{\partial \rho_i} + C(t) \end{aligned}$$

with boundary values $\rho(0) = \mu$ and $\rho(1) = \nu$. Here the discrete Hamiltonian is

$$\mathcal{H}(\rho, S) = \frac{1}{4} \sum_{i=1}^N \sum_{j \in N(i)} \frac{|S_i - S_j|^2}{(\delta x)^2} \theta_{ij}(\rho).$$

We observe that (2.2) is a semi-discrete version of the Wasserstein Hamiltonian flow, preserving the Hamiltonian and symplectic structure of the original system (1.2). Likewise, the Wasserstein distance $W(\mu, \nu)$ can be approximated by $\sqrt{2\mathcal{H}(\mu, S^0)}$, where S^0 is the initial condition of the spatially discrete S . Finally, define the density set by

$$\mathcal{P}(G) = \left\{ \rho = (\rho_i)_{i \in V} \left| \sum_{i \in V} \rho_i (\delta x)^d = 1, \rho_i \geq 0, i \in V \right. \right\},$$

137 where ρ_i represents the density on node i . The interior of $\mathcal{P}(G)$ is denoted by $\mathcal{P}_o(G)$.

138 In this study, (2.2) is the underlying spatial discretization for our numerical
139 method (but see (3.2) below), in large part because of the following result which
140 gives some important properties of (2.2), and whose proof is in [9, Proposition 2.1].

141 **PROPOSITION 2.1.** *Consider (2.2) with initial values μ and S^0 and let T^* be the
142 first time where the system develops a singularity. Then, for any $\mu \in \mathcal{P}_o(G)$ and any
143 function S^0 on V , there exists a unique solution of (2.2) for all $t < T^*$, and it satisfies
144 the following properties for all $t < T^*$.*

(i) *Mass is conserved:*

$$\sum_{i=1}^N \rho_i(t) = \sum_{i=1}^N \mu_i^0.$$

(ii) *Energy is conserved:*

$$\mathcal{H}(\rho(t), S(t)) = \mathcal{H}(\mu, S^0).$$

(iii) *Symplectic structure is preserved:*

$$d\rho(t) \wedge dS(t) = d\mu \wedge dS^0.$$

(iv) *The solution is time reversible: if $(\rho(t), S(t))$ is the solution of (2.2), then $(\rho(-t), -S(-t))$ also solves it.*

(v) *A time invariant $\tilde{\rho} \in \mathcal{P}_o(G)$ and $\tilde{S}(t) = -vt$ form an interior stationary solution of (2.2) if and only if $\mathcal{H}(\rho, S)$ is spatially independent (we denote it as $\mathcal{H}(\rho)$ in this case), $\tilde{\rho}$ is the critical point of $\min_{\rho \in \mathcal{P}_o(G)} \mathcal{H}(\rho)$ and $v = \mathcal{H}(\tilde{\rho})$.*

3. Algorithm. In this section, we first present the ideas of shooting methods, then combine them with a continuation strategy to design our algorithm for approximating the solution of the OT problem (1.1).

3.1. Single shooting. To illustrate the single shooting strategy, consider (2.2) in the time interval $[0, 1]$. Assuming that it exists, denote with $\rho(t, S^0)$, $t \in [0, 1]$, the solution of (2.2) with initial values (μ, S^0) . To satisfy the boundary value at $t = 1$, one needs to find S^0 such that the trajectory starting at (μ, S^0) passes through ν at $t = 1$, i.e.,

$$(3.1) \quad \rho(1, S^0) - \nu = 0.$$

To solve (3.1), root-finding algorithms must be used to update the current guess of S^0 to achieve better approximations. For example, when using Newton's method, the updates are supposedly computed by

$$J(1, S^{(i)}) \left(S^{(i+1)} - S^{(i)} \right) = -(\rho(1, S^{(i)}) - \nu), \quad i = 0, 1, \dots,$$

where $J(t, S) = \frac{\partial \rho(t, S)}{\partial S}$ is the Jacobian of $\rho(t, S) - \nu$ with respect to S . To ensure successful computations in Newton's method, finding a good initial guess for S^0 and having an invertible Jacobi matrix are crucial. But, as we anticipated in Remark 1.1, the Jacobian matrix $J(t, S)$ is singular, as otherwise a solution of (3.1) ought to be isolated, which can't be true, since adding an arbitrary constant will still give a solution.

To remedy this situation, we reverse to the (ρ, v) formulation, and rewrite the Hamiltonian system (2.2) into an equivalent form in terms of (ρ, v) . More precisely, by letting $v_{ij} = S_j - S_i$ for $ij \in E$, (2.2) becomes

$$(3.2) \quad \begin{aligned} \frac{d\rho_i}{dt} &= - \sum_{j \in N(i)} \frac{1}{(\delta x)^2} v_{ij} \theta_{ij}(\rho), \\ \frac{dv_{ij}}{dt} &= \frac{1}{2} \sum_{k \in N(j)} \frac{1}{(\delta x)^2} v_{kj}^2 \frac{\partial \theta_{jk}(\rho)}{\partial \rho_j} - \frac{1}{2} \sum_{k \in N(i)} \frac{1}{(\delta x)^2} v_{ki}^2 \frac{\partial \theta_{ik}(\rho)}{\partial \rho_i}. \end{aligned}$$

Since v_{ij} is the difference between S_j and S_i , a constant shift in S has no impact on the values of $v = \{v_{ij}\}$. On the other hand, there are now many redundant equations in (3.2), because $\{v_{ij}\}$ are not independent variables. For example, they must satisfy $v_{ij} = -v_{ji}$. Furthermore, there are total $N = (n+1)^d$ unknown values for S , while $2dn(n+1)^{d-1}$ unknowns for v on the lattice graph G . Clearly, to determine S up to a constant, only $N - 1$ values for v are needed. In other words, there must be only $N - 1$ independent v -equations in (3.2) to be solved, and the remaining ones are

181 redundant and must be removed so that the resulting system leads to a non-singular
 182 Jacobian.

183 There are different ways to remove the redundancies. To illustrate this in a simple
 184 setting, let us consider the 1-dimensional case ($d = 1$), in which the lattice graph G
 185 has $n - 1$ interior nodes and 2 boundary nodes. Each interior node has two neighbors
 186 while a boundary node has only one neighbor. We have at least two options: either
 187 to keep all equations for $v_{i,i+1}$, $i = 1, \dots, (N - 1)$, or to keep the equations for $v_{i,i-1}$,
 188 $i = 2, \dots, N$. Adopting the first choice, we have the following equations to solve

$$189 \quad (3.3) \quad \begin{aligned} \frac{d\rho_i}{dt} &= \frac{1}{(\delta x)^2} v_{(i-1)i} \theta_{(i-1)i}(\rho) - \frac{1}{(\delta x)^2} v_{i(i+1)} \theta_{i(i+1)}(\rho), \\ \frac{dv_{i(i+1)}}{dt} &= \frac{1}{4} \frac{1}{(\delta x)^2} v_{(i-1)i}^2 - \frac{1}{4} \frac{1}{(\delta x)^2} v_{i(i+1)}^2, \end{aligned}$$

190 for all $i = 1, \dots, N - 1$. If we take no-flux boundary conditions for (ρ, v) , we have
 191 $v_{01} = 0, \theta_{01} = 0$. Finally, mass conservation gives the condition $\rho_N = \frac{1 - \delta x \sum_{i=1}^{N-1} \rho_i}{\delta x}$.

192 Denoting $v(0) = v^0 = \{v_{i,i+1}^0\}_{i=1}^{N-1} = \{S_{i+1}^0 - S_i^0\}_{i=1}^{N-1}$, and the solution of (3.3)
 193 with initial values (μ, v^0) as $\rho_t = \rho(t, v^0)$, $v_t = v(t, v^0)$, we can revise the single shoot-
 194 ing strategy in terms of (ρ, v) as finding the initial velocity v^0 such that $\rho(1, v^0) = \nu$.
 195 By applying Newton's method, we obtain

$$196 \quad \hat{J}(1, v^{(m)})(v^{(m+1)} - v^{(m)}) = -(\rho(1, v^{(m)}) - \nu), \quad m = 0, 1, \dots,$$

where $\hat{J}(1, v^{(m)}) = \left[\frac{\partial \rho_t}{\partial v^0} \right]_{1, v^{(m)}}$ is the Jacobian of $\rho(t, v(0)) - \nu$ with respect to $v(0)$,
 evaluated at $t = 1$, $v = v^{(m)}$. For later reference, and since ν plays no role in the
 definition of \hat{J} , let us define the function

$$\hat{J}(t, v^0) = \left[\frac{\partial \rho}{\partial v^0} \right]_{t, v}, \quad t \geq 0.$$

198 Now, the single shooting strategy we just outlined is plagued by a common short-
 199 fall of single shooting techniques, namely that the initial guess $v^{(0)}$ must be quite close
 200 to the exact solution. In the present context, this is further exacerbated by the fact
 201 that (1.2) may develop singularities in finite time (see e.g. [9]), and as consequence
 202 the choice of a poor initial guess may (and does) lead to finite time blow-up of the
 203 solution of the initial value problem. To overcome this serious difficulty, we now give a
 204 result showing that the function $\hat{J}(t, v^0)$ remains invertible for sufficiently short times,
 205 and later will exploit this result to justify adopting a multiple shooting strategy.

206 **LEMMA 3.1.** *Let G be a 1-dimensional uniform lattice graph and let $t_1 > 0$ be
 207 sufficiently small. Assume that (ρ, v) is the smooth solution of (3.3) satisfying $\mu > 0$.
 208 Then, the function $\hat{J}(t, v^0)$ is invertible for $t \in (0, t_1]$.*

209 *Proof.* Direct calculation shows that the function $\hat{J}(t, v^0) = \frac{\partial}{\partial v^0} \rho(t, v^0)$ satisfies

$$210 \quad \begin{aligned} \frac{d}{dt} \frac{\partial \rho_t}{\partial v^0} &= B_{11} \frac{\partial v_t}{\partial v^0} + B_{12} \frac{\partial \rho_t}{\partial v^0}, \quad \hat{J}(0, v^0) = 0_{n \times n}, \\ 211 \quad \frac{d}{dt} \frac{\partial v_t}{\partial v^0} &= B_{22} \frac{\partial v_t}{\partial v^0}, \quad \left[\frac{\partial v_t}{\partial v^0} \right]_{t=0} = I, \end{aligned}$$

213 where

$$214 \quad (B_{11})_{ii} = -\frac{\rho_i + \rho_{i+1}}{2(\delta x)^2}, \quad i = 1, \dots, n - 1,$$

$$\begin{aligned}
215 \quad (B_{11})_{i,i-1} &= \frac{\rho_i + \rho_{i-1}}{2(\delta x)^2}, i = 2, \dots, n, \\
216 \quad (B_{11})_{nn} &= \frac{1 - \sum_{i=1}^{n-1} \rho_i \delta x}{2(\delta x)^3}, \\
217 \quad (B_{12})_{11} &= -\frac{v_1}{2(\delta x)^2}, (B_{12})_{ii}(\rho, v) = -\frac{v_i}{2(\delta x)^2} + \frac{v_{i-1}}{2(\delta x)^2}, i = 2, \dots, n, \\
218 \quad (B_{12})_{i,i-1} &= \frac{v_{i-1}}{2(\delta x)^2}, (B_{12})_{i,i+1} = -\frac{v_i}{2(\delta x)^2}, i = 2, \dots, n-1, \\
219 \quad (B_{12})_{n,i} &= \frac{v_n}{2(\delta x)^2}, i = 1, \dots, n-2, (B_{12})_{n,n-1} = \frac{v_n}{2(\delta x)^2} + \frac{v_{n-1}}{2(\delta x)^2}, \\
220 \quad (B_{22})_{i,i+1} &= -\frac{1}{2(\delta x)^2} v_{i+1}, i = 1, \dots, n-1, (B_{22})_{i,i-1} = \frac{1}{2(\delta x)^2} v_{i-1}, i = 2, \dots, n.
\end{aligned}$$

Since B_{11} is a lower triangular matrix, it is invertible if and only if

$$\min_{i \leq n}(\theta_{i,i+1}(\rho)) > 0,$$

222 where θ_{ij} is defined in (2.1) and hence $\theta_{i,i+1}(\rho) > 0$ for as long as ρ remains positive.
223 Moreover, given the initial condition to the identity for $\frac{\partial v_t}{\partial v^0}$, if $t_1 > 0$ is sufficiently
224 small the matrix $\frac{\partial v_t}{\partial v^0}$ remains invertible. Furthermore, since $\hat{J}(0, v^0) = 0_{n \times n}$, we
225 conclude that for $t > 0$ sufficiently small

$$226 \quad \hat{J}(t, v^0) \approx t B_{11} + \mathcal{O}(t^2),$$

227 which implies that $\hat{J}(t, v^0)$ is invertible for $t > 0$, and sufficiently small. \square

228 Once v values become available, if desired we can reconstruct S on the lattice
229 graph G from the relation $v_{ij} = S_i - S_j$.

230 We conclude this section by emphasizing that the semi-discretization (3.2) is
231 a spatial discretization of the Wasserstein geodesic equations written in term of
232 (ρ, v) [9]. However, this semi-discretization has been arrived at by designing a semi-
233 discretization scheme for the system (1.2) in the (ρ, S) variables, respecting the Hamiltonian
234 nature of the problem, see (2.2) and Proposition 2.1.

235 **3.2. Multiple shooting method.** As proved in Lemma 3.1, in the 1-d case the
236 function $\hat{J}(t, v^0)$ is invertible for sufficiently short times; however, for the success of
237 single shooting, this ought to be invertible at $t = 1$, a fact which is often violated. In
238 addition, our numerical experiments indicate poor stability behavior when using the
239 single shooting method to solve the Wasserstein geodesic equations (2.2). To mitigate
240 these drawbacks, we propose to use multiple shooting.

241 We partition the interval $[0, 1]$ into the union of sub-intervals $[t_k, t_{k+1}], k = 0, \dots, K-1$, and let $\delta t = \max_k(t_{k+1} - t_k)$. For example, we could take $t_k = k\delta t$ and
242 $K\delta t = 1$. To illustrate, we again take G as the d-dimensional uniform lattice graph.
243 In each subinterval $[t_k, t_{k+1}], k = 0, \dots, K-1$, (2.2) is converted into equations in
244 terms of (ρ, v) , just like the ones in (3.2),

$$\begin{aligned}
246 \quad \frac{d\rho_i^{k+1}}{dt} &= -\sum_{j \in N(i)} \frac{1}{(\delta x)^2} v_{ij}^{k+1} \theta_{ij}(\rho), \\
247 \quad \frac{dv_{ij}^{k+1}}{dt} &= \frac{1}{2} \sum_{l \in N(j)} \frac{1}{(\delta x)^2} (v_{jl}^{k+1})^2 \frac{\partial \theta_{lj}(\rho)}{\partial \rho_j} - \frac{1}{2} \sum_{m \in N(i)} \frac{1}{(\delta x)^2} (v_{mi}^{k+1})^2 \frac{\partial \theta_{ik}(\rho)}{\partial \rho_i},
\end{aligned}$$

248

where $i \in N$ is a multi-index for a grid point in d-dimensional lattice. The super script $k + 1$ in ρ and v indicates that the corresponding variables are defined in the subinterval $[t_k, t_{k+1}]$. Then, the multiple shooting method requires finding the values of ρ, v at temporal points $\{t_k\}_{k=0}^{K-1}$, i.e.,

$$(\tilde{v}^0, \tilde{\rho}^1, \tilde{v}^1, \dots, \tilde{\rho}^{K-1}, \tilde{v}^{K-1})^T,$$

249 such that the continuity conditions hold, that is, for $k = 0, \dots, K - 2$,

$$F_{2k+1}(\tilde{\rho}^k, \tilde{v}^k, \tilde{\rho}^{k+1}) = \rho^{k+1}(t_{k+1}, \tilde{\rho}^k, \tilde{v}^k) - \tilde{\rho}^{k+1} = 0,$$

$$F_{2k+2}(\tilde{\rho}^k, \tilde{v}^k, \tilde{v}^{k+1}) = v^{k+1}(t_{k+1}, \tilde{\rho}^k, \tilde{v}^k) - \tilde{v}^{k+1} = 0.$$

253 When $k = 0$ and $k = K - 1$, the given boundary values $\rho(0) = \mu$ and $\rho(1) = \nu$ yield
254 that

$$F_1(\mu, \tilde{v}^0, \tilde{\rho}^1) = \rho^1(t_1, \mu, \tilde{v}^0) - \tilde{\rho}^1 = 0,$$

$$F_{2K-1}(\tilde{\rho}^{K-1}, \tilde{v}^{K-1}, \nu) = \rho^K(t_K, \tilde{\rho}^{K-1}, \tilde{v}^{K-1}) - \nu = 0.$$

255 As customary, we use Newton's method to find the root $(\tilde{v}^0, \tilde{\rho}^1, \tilde{v}^1, \dots, \tilde{\rho}^{K-1}, \tilde{v}^{K-1})$
256 of $F = (F_w)_{w=1}^{2K-1} = 0$. To this end, we first need to remove the redundant equations
257 for the velocity field v . The number of unknown variables in ρ is $N - 1 = (n + 1)^d - 1$,
258 which is one fewer than the total number of nodes in G , because the total probability
259 must be one. The number of unknowns in S is N . The vector field v contains the
260 differences in S , hence the total number of independent variables in v is also $N - 1$,
261 due to the connectivity of G . The following lemma ensures that we can always find
262 the $N - 1$ components of v from which one can generate all the components of v on
263 the lattice graph G .

264 **LEMMA 3.2.** *Given a connected d-dimensional lattice graph G and a vector field
265 v which is generated by a potential S on G , there exists a subset consisting of $N - 1$
266 components of v , denoted by $\hat{v} = (\hat{v}_w)_{w=1}^{N-1}$, such that any v_{ij} can be expressed as
267 combination of the entries of \hat{v} , i.e.*

$$268 \quad (3.4) \quad v_{ij} = \sum_{w=1}^{N-1} a_w \hat{v}_w, \quad \text{where } a_w = 1, \text{ or } -1, \text{ or } 0.$$

269 *Proof.* Since G is connected, there is always a path on the graph passing through
270 all the nodes of G and with exactly $N - 1$ edges. We denote with \hat{v}_i the value of v on
271 the i -th edge along the path. By definition of $v_{ij} = S_j - S_i$, the values of S can be
272 reconstructed, up to a constant shift, along the path. Therefore, all entries of v can
273 be expressed as the above combination of the entries $(\hat{v}_w)_{w=1}^{N-1}$. \square

274 From the proof, we observe that the choice of \hat{v} is not unique, since every path
275 going through all nodes of G using $N - 1$ edges will give a system with no redundancy.
276 The edges could be passed multiple times. Let us select one such choice and denote
277 it by $(\hat{v}_w)_{w=1}^{N-1}$. For instance, in 2-dimensional lattice graph G , we choose the \hat{v}
278 that generates the vector field (see Fig. 3.1) as follows. Denote every node on G
279 by $(i, j)_{i,j=1}^{n+1}$. For fixed i , $(i, j)_{i,j=1}^{n+1}$ becomes 1-dimensional lattice graph in the x_2
280 direction. Following (3.3), we choose $\hat{v}_w = v_{(i,j)(i,j+1)}$ for $w = n \times (i - 1) + j$,
281 $j = 1, \dots, n, i = 1, \dots, n + 1$, which gives $(n + 1) \times n$ components of \hat{v}_w . Because of
282

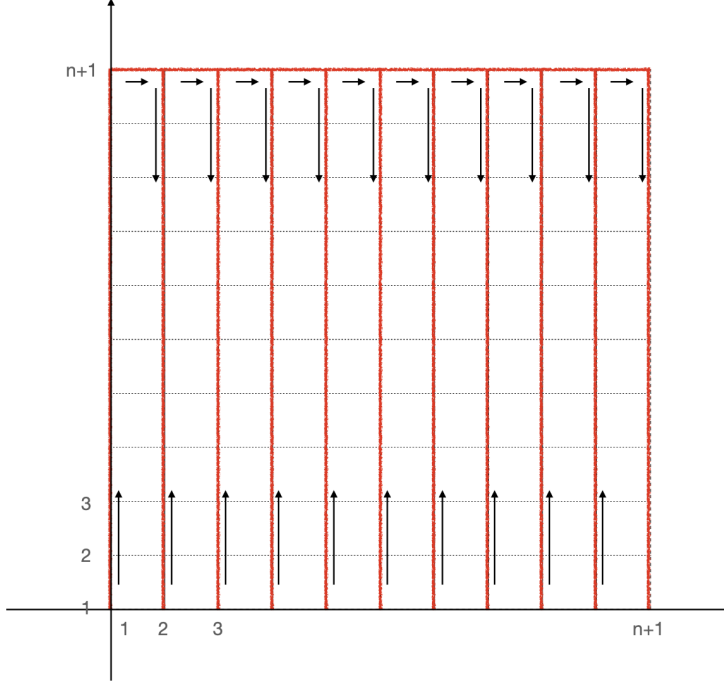


FIG. 3.1. The edges (in red) of \hat{v} that generates of the velocity in 2D lattice graph. The path is indicated by the arrows. Clearly, many edges are passed twice.

286 the connectivity of G relative to the x_1 direction, the last n components of \hat{v}_w are
 287 chosen by $\hat{v}_w = v_{(j,1)(j+1,1)}$, for $w = (n+1) \times n + j$, $j = 1, \dots, n$. For convenience, let
 288 us denote the velocity on the related edges in this path by $\{v_{i_w i_{w+1}}\}_{w=1}^{N-1} = \{\hat{v}_w\}_{w=1}^{N-1}$.
 289 Then the reduced Wasserstein system (2.2) becomes

$$\begin{aligned}
 \frac{d\rho_{i_w}^{k+1}}{dt} &= \sum_{j \in N(i_w)} v_{j i_w}^{k+1} \theta_{i_w j}(\rho), \\
 290 \quad (3.5) \quad \frac{d\hat{v}_{i_w}^{k+1}}{dt} &= \frac{1}{2} \sum_{j \in N(i_w)} \frac{1}{(\delta x)^2} (v_{i_w, j}^{k+1})^2 \frac{\partial \theta_{i_w j}(\rho)}{\partial \rho_{i_w}} \\
 &\quad - \frac{1}{2} \sum_{m \in N(i_{w+1})} \frac{1}{(\delta x)^2} (v_{i_{w+1}, m}^{k+1})^2 \frac{\partial \theta_{i_{w+1} j}(\rho)}{\partial \rho_{i_{w+1}}},
 \end{aligned}$$

291 where v_{ij} satisfies (3.4) and the unknowns are (ρ, \hat{v}) with

$$\begin{aligned}
 292 \quad \rho^{k+1}(t_k, \rho(t_k), \hat{v}(t_k)) &= \rho(t_k), \quad \rho^{k+1}(t_{k+1}, \rho(t_k), \hat{v}(t_k)) = \rho(t_{k+1}), \\
 293 \quad \hat{v}^{k+1}(t_k, \rho(t_k), \hat{v}(t_k)) &= \hat{v}(t_k), \quad \hat{v}^{k+1}(t_{k+1}, \rho(t_k), \hat{v}(t_k)) = \hat{v}(t_{k+1}).
 \end{aligned}$$

295 We apply the multiple shooting method to (3.5), i.e., we look for the root $Z =$

296 $(\hat{v}^0, \rho^1, \hat{v}^1, \dots, \rho^{K-1}, \hat{v}^{K-1})$ of F defined by

$$\begin{aligned} F_{2k+1}(\rho^k, \hat{v}^k, \rho^{k+1}) &= \rho^{k+1}(t_{k+1}, \rho^k, \hat{v}^k) - \rho^{k+1} = 0, \\ 297 \quad (3.6) \quad F_{2k+2}(\rho^k, \hat{v}^k, \hat{v}^{k+1}) &= \hat{v}^{k+1}(t_{k+1}, \rho^k, \hat{v}^k) - \hat{v}^{k+1} = 0, \quad k \leq K-2, \\ F_{2K-1}(\rho^{K-1}, \hat{v}^{K-1}, \rho^K) &= \rho^K(t_{K-1}, \rho^{K-1}, \hat{v}^{K-1}) - \nu = 0, \end{aligned}$$

298 where $\rho^0 = \mu, \rho^K = \nu$.

299 Use of Newton's method to solve (3.6) gives

$$300 \quad (3.7) \quad A^{(m)} \Delta Z^{(m)} = -F^{(m)},$$

where m is the iteration index, $\Delta Z^{(m)} = Z^{(m+1)} - Z^{(m)}$,

$$Z^{(m)} = (v^{0,(m)}, \rho^{1,(m)}, v^{1,(m)}, \dots, v^{K-1,(m)}, \rho^{K-1,(m)})^T,$$

$F^{(m)} = (F_1(Z^{(m)}), F_2(Z^{(m)}), \dots, F_{2K-1}(Z^{(m)}))^T$, and $A^{(m)}$ is the Jacobian of F , whose structure is as follows, where the X correspond to nonzero $(N-1) \times (N-1)$ matrices:

$$\begin{pmatrix} X & X & 0 & 0 & 0 \\ X & 0 & X & 0 & 0 \\ 0 & X & X & X & 0 \\ 0 & X & X & 0 & X \\ & & X & X & X & 0 \\ & & X & X & 0 & X \\ & & & & \ddots & \ddots \\ & & & & X & X & X & 0 \\ & & & & X & X & 0 & X \\ & & & & X & X & X & X \end{pmatrix}.$$

302 Omitting the superscript m in the expressions of $A^{(m)}$, the blocks $A_{ij}, i, j = 1, \dots, 2K-1$, are easily seen to be the following. For $i = 2, \dots, K-1$,

$$304 \quad A_{2(i-1)+1, 2(i-1)} = \frac{\partial \rho^i(t_i, v^{i-1}, \rho^{i-1})}{\partial v^{i-1}}, \quad A_{2(i-1)+1, 2(i-1)+1} = \frac{\partial \rho^i(t_i, v^{i-1}, \rho^{i-1})}{\partial \rho^{i-1}},$$

$$305 \quad A_{2i, 2(i-1)} = \frac{\partial v^i(t_i, v^{i-1}, \rho^{i-1})}{\partial v^{i-1}}, \quad A_{2i, 2(i-1)+1} = \frac{\partial v^i(t_i, \rho^{i-1}, \rho^{i-1})}{\partial \rho^{i-1}},$$

$$306 \quad A_{2(i-1)+1, 2i} = -I, \quad A_{2i, 2i+1} = -I,$$

$$307 \quad A_{11} = \frac{\partial \rho^1(t_1, v^0)}{\partial v^0}, \quad A_{12} = -I,$$

$$308 \quad A_{21} = \frac{\partial v^1(t_1, v^0)}{\partial v^0}, \quad A_{23} = -I,$$

310 and

$$311 \quad A_{2K-1, 2K-2} = \frac{\partial \rho^K(t_K, v^{K-1}, \rho^{K-1})}{\partial v^{K-1}}, \quad A_{2K-1, 2K-1} = \frac{\partial \rho^K(t_K, v^{K-1}, \rho^{K-1})}{\partial \rho^{K-1}}.$$

313 Below we show invertibility of $A^{(m)}$ for δt sufficiently small.

314 THEOREM 3.1. Let (ρ, v) be the unique solution of (3.2) and $Z^* = (v(0), \rho(t_1),$
315 $v(t_1), \dots, \rho(t_{K-1}), v(t_{K-1}))^T$ be the exact solution evaluated at the multiple shooting

316 points. Assume that the initial vector $Z^{(0)}$ is sufficiently close to Z^* , i.e., $|Z^{(0)} - Z^*| = \mathcal{O}(\epsilon)$ for $\epsilon > 0$ sufficiently small, (ρ, v) is continuously differentiable in $[0, 1]$
 317 satisfying $(\rho, v) \in \mathcal{C}_b^2([0, 1]; \mathbb{R}^N) \times \mathcal{C}_b^2([0, 1]; \mathbb{R}^N \times \mathbb{R}^N)$ and $\min_{t \in [0, T]} \min_{i=1}^N \rho_i \geq c > 0$, and
 318 that $\frac{\partial \rho(1, \rho^0, v^0)}{\partial v^0}$ is invertible. Then, Newton's method of the multiple shooting method
 319 (3.7) is quadratically convergent to Z^* for δt sufficiently small.

321 *Proof.* By standard Newton's convergence theory, it will be enough to prove the
 322 invertibility of Jacobian matrix $A^{(0)}$ for appropriately small ϵ and δt . Rewrite $A^{(0)}$ in
 323 partitioned form $\begin{pmatrix} A'_{11} & A'_{12} \\ O_{N-1, N-1} & A'_{22} \end{pmatrix}$, where A'_{11} is a $(2K-2)n \times n$ matrix, A'_{12} is a
 324 $(2K-2)n \times (2K-2)n$ matrix, and A'_{22} is a $(N-1) \times (2K-2)(N-1)$ matrix. Using
 325 the property of determinant for the partitioned matrix and the fact that $\det(A'_{12}) = 1$,
 326 and writing A in lieu of $A^{(0)}$, we have

$$\begin{aligned} 327 \quad \det(A) &= \det \begin{pmatrix} 0_{N-1 \times N-1} & A'_{22} \\ A'_{11} & A'_{12} \end{pmatrix} \\ 328 &= \det(A'_{12}) \det(0_{N-1 \times N-1} - A'_{22}(A'_{12})^{-1} A'_{11}) \\ 329 &= (-1)^{N-1} \det(A'_{22}(A'_{12})^{-1} A'_{11}). \end{aligned}$$

331 So, we are left to show that $\det(A'_{22}(A'_{12})^{-1} A'_{11}) \neq 0$. The structure of A'_{12} implies
 332 that

$$\begin{aligned} 333 \quad A'_{22}(A'_{12})^{-1} A'_{11} &= \left(\frac{\partial \rho^{K, (0)}}{\partial \rho^{K-1, (0)}}, \frac{\partial \rho^{K, (0)}}{\partial v^{K-1, (0)}} \right) \\ &\quad \prod_{i=2}^{K-1} \left(\begin{pmatrix} \frac{\partial \rho^{i, (0)}}{\partial \rho^{i-1, (0)}} & \frac{\partial \rho^{i, (0)}}{\partial v^{i-1, (0)}} \\ \frac{\partial v^{i, (0)}}{\partial \rho^{i-1, (0)}} & \frac{\partial v^{i, (0)}}{\partial v^{i-1, (0)}} \end{pmatrix} \left(\frac{\partial \rho^{1, (0)}}{\partial v^{0, (0)}}, \frac{\partial v^{1, (0)}}{\partial v^{0, (0)}} \right)^T, \right. \end{aligned}$$

334 where $\rho^{i, (0)} = \rho^i(t_K, \rho^{i-1, (0)}, v^{i-1, (0)})$, $v^{i, (0)} = v^k(t_K, \rho^{i-1, (0)}, v^{i-1, (0)})$, for $i = 2, \dots, K$, and $v^{1, (0)} = v^1(t_1, v^{0, (0)})$, $\rho^{1, (0)} = \rho^1(t_1, v^{0, (0)})$.

335 Now, invertibility of the Jacobian matrix A (or $A'_{22}(A'_{12})^{-1} A'_{11}$) follows from
 336 invertibility of the Jacobian matrix at the exact solution $\frac{\partial \rho(t_K, \rho^0, v^0)}{\partial v^0}$. To see this, due
 337 to (3.8), the continuous differentiability of the exact solution, and the assumption
 338 that $|Z^{(0, (m))} - Z^*| = \mathcal{O}(\epsilon)$, we have that

$$340 \quad A'_{22}(A'_{12})^{-1} A'_{11} = \frac{\partial \rho(t_K, \rho^0, v^0)}{\partial v^0} + \mathcal{O}(\epsilon) + \mathcal{O}(\delta t).$$

341 Therefore, the invertibility of $\frac{\partial \rho(t_K, \rho^0, v^0)}{\partial v^0}$ with $t_K = 1$ implies the invertibility of the
 342 Jacobian matrix A . Combining with the assumption that ϵ and δt are sufficiently
 343 small, we obtain that $A^{(0)}$ is invertible in a neighborhood of Z^* , which, together with
 344 the boundedness assumption on ρ, v , implies the quadratic convergence of Newton's
 345 method. \square

346 **REMARK 3.1.** Of course, the initial value problems for the multiple shooting method
 347 must be integrated numerically. We have not accounted for this in Theorem 3.1. In
 348 principle, many choices are available to integrate these initial value problems; we have
 349 used the symplectic integrators developed in [9] for Wasserstein Hamiltonian flows,
 350 without regularization by Fisher information.

352 **3.3. Continuation multiple shooting strategy.** In light of Theorem 3.1, and
 353 notwithstanding the need for small δt , the multiple shooting method requires the
 354 initial guess to be near the exact solution Z^* . To make the method robust with
 355 respect to the initial guess, we adopt a standard continuation strategy by introducing
 356 a density function $f(\mu, \nu, \lambda)$, which is smooth with respect to a homotopy parameter
 357 $\lambda \in [0, 1]$ and satisfies

358 (3.8) $f(\mu, \nu, 0) = \mu, \quad f(\mu, \nu, 1) = \nu.$

360 The specific choice of f in (3.8) depends on the initial and terminal distributions μ
 361 and ν . We illustrate below with two typical situations.

(a) “Gaussian-type” densities. If $\mu(x) = K_0 \exp(-c|x - b_0|^2)$ and $\nu(x) = K_1 \exp(-c|x - b_1|^2)$, with $\int_{\mathcal{O}} \mu dx = \int_{\mathcal{O}} \nu dx = 1$, we choose

$$f(\mu, \nu, \lambda)(x) = K_\lambda \exp(-c|x - b_0 - \lambda(b_1 - b_0)|^2)$$

with K_λ chosen so that $\int_{\mathcal{O}} f dx = 1$. For $\mu = K_0 \exp(-c_0|x - b_0|^2), \nu = K_1 \exp(-c_1|x - b_1|^2)$, we choose

$$f(\mu, \nu, \lambda)(x) = K_\lambda \exp(-(c_0 + \lambda(c_1 - c_0))|x - b_0 - \lambda(b_1 - b_0)|^2)$$

362 with K_λ chosen so that $\int_{\mathcal{O}} f dx = 1$.

(b) For general μ and ν , we choose f as the linear interpolant of μ and ν , which
 is automatically normalized. That is, we take

$$f(\mu, \nu, \lambda) = (1 - \lambda)\mu + \lambda\nu.$$

363 REMARK 3.2. For the success of our method, it is actually important that the
 364 densities be strictly positive (see Theorem 3.1). For this reason, and especially when
 365 the densities μ and ν are exponentially decaying (like Gaussians do), we add a small
 366 positive number, which we call shift, to the densities μ and ν and re-scale them so to
 367 keep the total probabilities equal to 1. In the numerical tests in Section 4, these are
 368 the values r_0 and r_1 we use.

369 Using f , we consider the system (3.5) with λ dependent boundary conditions
 370 given by $\rho(0) = \mu$ and $\rho(1) = f(\mu, \nu, \lambda)$. Obviously, the problem with $\lambda_0 = 0$ is trivial
 371 to solve (the identity map), and it can be used as initial guess for the solution at
 372 the value $\lambda_1 = \Delta\lambda$. By gradually increasing λ from 0 to 1, we eventually obtain the
 373 solution for (2.2) with boundary conditions μ and ν , which is the original Wasserstein
 374 geodesic problem we wanted to solve. This basic idea to use the solution with smaller
 375 value of λ as the initial guess for the boundary value problem with larger value of
 376 λ is well understood, and universal. In our context, it is important to note that it
 377 works because of OT problem always has an optimal map as long as μ and $f(\mu, \nu, \lambda)$
 378 satisfy $\int_{\mathbb{R}^d} |x|^2 \mu dx, \int_{\mathbb{R}^d} |x|^2 f(\mu, \nu, \lambda) dx < +\infty$ (e.g., see [25]). In turns, this implies
 379 the existence of v or S (up to ρ_t -measure 0 sets) for the BVP problem. In particular,
 380 this fact guarantees that there is a finite sequence $\{\lambda_j\}_{j \leq L}$, $\lambda_L = 1$, and $Z_{\lambda_L}^*$ will be
 381 our approximation to the exact solution (ρ, v) at the multiple shooting points.

382 (3.9) $Z_{\lambda_0}^0 := (v^{0,(0)}, \rho^{1,(0)}, \dots, v^{K-1,(0)}, \rho^{K-1,(0)})^T.$

384 For instance, we may take $v^{k,(0)}, k \leq K-1$, as constant vectors, $\rho^{k,(0)}, k \leq K-1$,
 385 from linear interpolation of $\rho^0 = \mu$ and $\rho^1 = f(\mu, \nu, \lambda_0)$, i.e.,

386 $\rho^{k,(0)} = t_k \mu + (1 - t_k) f(\mu, \nu, \lambda_0), k \leq K-1.$

387

388 Finally, throughout all of our experiments, we enforced the following stopping
 389 criterion for the Newton iteration:

$$390 \quad (3.10) \quad \frac{|F(Z^{(m+1)}) - F(Z^{(m)})|}{F(Z^{(m)})} < 10^{-5}.$$

391 We summarize the steps in the following algorithm.

Algorithm 3.1

Input: Multiple shooting points t_k , $k = 0, \dots, K$, with $t_0 = 0$ and $t_K = 1$. Discrete densities μ , ν , on the spatial grid of size δx , continuation parameter λ , max-number of Newton's iterations **Maxits**.

Output: The minimizer Z^* at the multiple shooting points;

- 1: Follow (3.9) and produce a initial guess $Z_{\lambda_0}^{(0)}$;
- 2: Until $\lambda_j = 1$ or too many continuation steps, **do**
- 3: **for** $m = 1, 2, \dots, \text{Maxits}$, while (3.10) not satisfied **do**
- 4: Solve $J_{\lambda_j}^{(m)} d^{(m)} = -F(Z_{\lambda_j}^{(m)})$;
- 5: $Z_{\lambda_j}^{(m+1)} = Z_{\lambda_j}^{(m)} + d^{(m)}$;
- 6: **end for**
- 7: $\lambda_{j+1} = \lambda_j + \Delta\lambda$ (see Remark 3.5);
- 8: put $Z_{\lambda_{j+1}}^0 = Z_{\lambda_j}^*$ as the new initial guess;
- 9: $j + 1 \rightarrow j$, go back to step 2.

392 REMARK 3.3. *Based on the output of Algorithm 3.1, the Wasserstein distance (or*
 393 *the Hamiltonian of (2.2)) can be easily obtained. From the first component $v^{0,*}$ of*
 394 *Z^* , we can reconstruct the initial values for S^0 as follows. The first component $v^{0,*} =$*
 395 *$(\hat{v}_w)_{w=1}^{N-1}$, $\{i_w i_{w+1}\}_{w=1}^{N-1}$ generates the initial vector field. We first define the potential*
 396 *S on a fixed node i_0 . Due to the connectivity of G , using $S_{i_{w+1}} = v_{i_w, i_{w+1}} + S_{i_w}$, we*
 397 *get the other initial values of S^0 . Then the Wasserstein distance can be evaluated as*
 398 *$W(\mu, \nu) = \sqrt{2H(\mu, S^0)}$.*

399 REMARK 3.4 (Barrier value for density). *On rare occasions, we observed that*
 400 *during the Newton's iteration the updates became negative, leading to a failure. To*
 401 *avoid this phenomenon, we adopted a simple strategy, whereby we created a barrier*
 402 *for the values of the densities, and reset to this barrier any value which went below it.*
 403 *In our tests in Section 4, use of this artifical barrier was needed only for Examples 4.6*
 404 *and 4.11. To witness, in Example 4.6, we used the barrier at 10^{-5} , and in Example*
 405 *4.11 the barrier was set at 10^{-3} . Clearly with this strategy the total mass of the*
 406 *numerical solution is not exactly equal to 1, but the error incurred in the total mass*
 407 *is at the same level of the barrier value.*

408 REMARK 3.5 (Choosing continuation steps). *We implemented a very simple and*
 409 *conservative continuation strategy. In all of our tests, we first try to take $\lambda = 1$, to*
 410 *see whether the continuation is really needed. If the method does not work without*
 411 *continuation, we begin with a value λ_0 of λ for which multiple shooting works (e.g.,*
 412 *we usually take $\lambda_0 = 0.1$ as initial step), and choose a value $\Delta\lambda = \frac{1-\lambda_0}{L}$ with given L*
 413 *(e.g., $L = 10$ or 20 is our usual choice). We then try to continue by taking steps of*
 414 *size $\Delta\lambda$, though if the Newton's multiple shooting fails we decrease $\Delta\lambda$ by dividing the*
 415 *remaining interval by L again and/or increase the value of L by doubling it. In all*
 416 *tests of Section 4, except Examples 4.1 and 4.5, the continuation strategy was needed.*

dx	Maximum Error	L^2 -Error	Iterations
1/16	0.00120	0.00068	4
1/32	0.00057	0.00034	5
1/64	0.00003	0.00017	6
1/128	0.000019	0.000086	11

TABLE 1
The error in the velocity for Example 4.1

417 REMARK 3.6 (Choosing homotopy $f(\mu, \nu, \lambda)$). *Finally, for all tests with Gaussian type densities μ, ν , we use the Gaussian interpolation (a) in subsection 3.3 for $f(\mu, \nu, \lambda)$. For other examples, we use the linear interpolation (b) in subsection 3.3 for $f(\mu, \nu, \lambda)$. To exemplify, in Example 4.6, we take $f(\mu, \nu, \lambda)$ as the normalization of $\exp(-5(x_2 - 0.5 - 1.95\lambda)^2 - 5(x_1 - 1.5 - 0.95\lambda)^2) + \exp(-5(x_2 - 0.5 - 1.95\lambda) - 5(x_1 - 1.5 + 0.95\lambda))^2 + r$ and obtain a sequence of λ 's starting from $\lambda_0 = 0.1$, with $\Delta\lambda = 0.9/20$.*

424 **4. Numerical experiments.** In this section, we apply Algorithm 3.1 to approximate the solution of several OT problems. Throughout the experiments, the Jacobian in Newton's method is approximated by using a 1st order divided difference approximation of the derivatives. The spatial boundary conditions for the density functions are set to be homogeneous Neumann boundary conditions for all experiments except for Example 4.1, which is subject to periodic boundary conditions. Except for this Example 4.1, we do not have the exact solutions of our test problems, so we display the evolution of the density from μ to ν as indication of the quality of the approximation.

EXAMPLE 4.1. *Here the spatial domain is the 2-torus $\mathbb{T}^2 = [0, 1] \times [0, 1]$, subject to periodic boundary conditions. Following the approach in [25], we define a smooth function $\phi(x_1, x_2) = \beta \sin(2\pi x_1) \sin(2\pi x_2)$, with $\beta = \frac{1}{64}(2\pi)^{-2}$, take initial density $\mu(x_1, x_2) = \det(I - D^2\phi(x_1, x_2))$ and target density ν is the uniform distribution on \mathbb{T}^2 . In this case, the exact initial velocity can be explicitly given:*

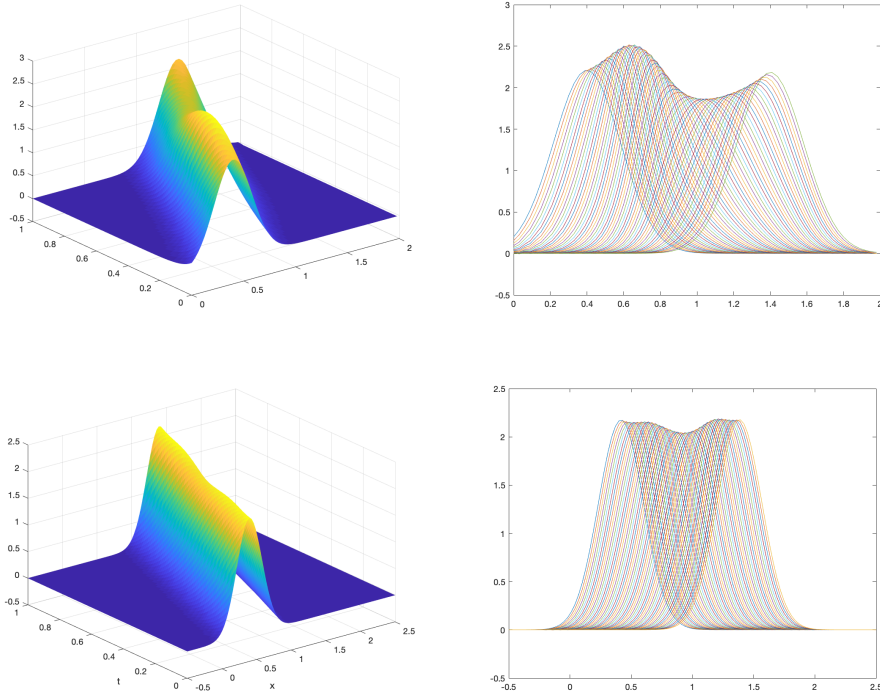
$$v^0(x_1, x_2) = 2\pi\beta(\cos(2\pi x_1) \sin(2\pi x_2), \sin(2\pi x_1) \cos(2\pi x_2)),$$

433 *and in Table 1 we measure the approximation error of our method, with respect to the spatial grid-size. As it turns out, this was a very easy problem to solve, and single shooting with a quasi-Newton approach (only one Jacobian matrix was computed and factored and then used across all iterations) solved it adequately. There was no need of adopting a continuation strategy, and we took 160 integration steps from 0 to 1. About 90% of the computation time was spent on calculating the Jacobian at the initial guess. From Table 1, we observe 1st order convergence with respect to both L^2 and sup norms, i.e., $\|\hat{v}^0 - v^0\|_{l^\infty}, \|\hat{v}^0 - v^0\|_{L^2}$, where \hat{v} is the initial function on the grids solved by single shooting method, and l^∞, L^2 denote the discrete sup norm and L^2 norm respectively. This is in agreement with the semi-discretization scheme we used.*

443 **4.1. 1D numerical experiments.** Below we present results on 1-D OT problems, with one or both densities of Gaussian types. Namely, the initial and terminal distributions μ and ν are normalizations of

$$446 \quad (4.1) \quad \hat{\mu} = \exp(-a_0(x - b_0)^2) + r_0, \quad \hat{\nu} = \exp(-a_1(x - b_1)^2) + r_1,$$

447 *scaled so that $\int_{\mathcal{O}} \mu dx = \int_{\mathcal{O}} \nu dx = 1$. (Here, \mathcal{O} is a subinterval of the real line.)*

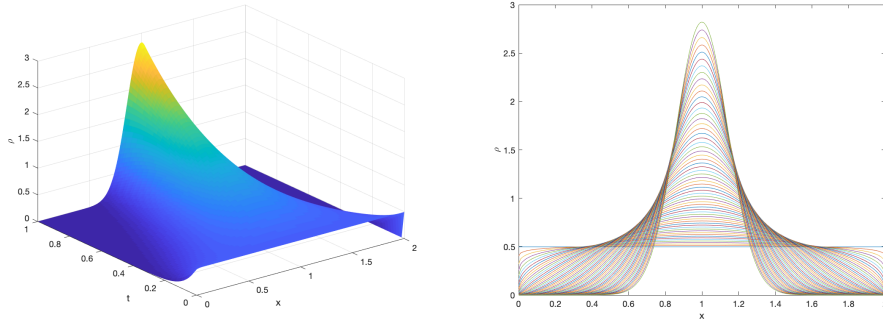
FIG. 4.1. Example 4.2: evolution of $\rho(t)$ for truncated interval $[0, 2]$ (top) and $[-0.5, 2.5]$ (bottom).

448 EXAMPLE 4.2. Here we look at the performance of the multiple shooting method
 449 when varying the (truncation of the real line to the) finite interval \mathcal{O} , and the shift
 450 number r . The parameters of initial and terminal distributions μ, ν in (4.1) are $a_0 =$
 451 $a_1 = 15, b_0 = 0.4, b_1 = 1.4$. We take $K = 60$ multiple shooting points, spatial step
 452 size $dx = 3 \times 10^{-2}$, $N = 300$ time steps per subinterval, $r_0 = r_1 = 0.0001$ in (4.1),
 453 and consider the intervals $\mathcal{O} = [0, 2]$ or $[-0.5, 2.5]$. In Fig. 4.1, we plot the evolution
 454 of density. The top figures refer to $\mathcal{O} = [0, 2]$ and show distortion in the density
 455 evolution. The bottom row refers to $\mathcal{O} = [-0.5, 2.5]$ and shows that the computation
 456 is more faithful when the truncated domain is large enough.

457 EXAMPLE 4.3. Here $\mathcal{O} = [0, 2]$, the initial distribution is the uniform distribution
 458 $\mu = \frac{1}{2}$ and the terminal distribution ν is the normalized Gaussian density as the $\hat{\nu}$
 459 used in Example 4.2 with $a_1 = 25, b_1 = 1, r_1 = 0$. The number of multiple shooting
 460 points is $K = 60$, the space stepsize $dx = 5 \times 10^{-2}$ and we take $N = 20$ integration
 461 steps for subinterval. Fig. 4.2 shows the density evolution.

462 REMARK 4.1. In general, we observed that when we refine the spatial step size,
 463 the number of multiple shooting subintervals must increase in order to maintain non-
 464 negativity of the density at the temporal grids, and a successful completion of our
 465 multiple shooting method, whereas the number of integration steps on each subinterval
 466 is not as critical. See Table 2 for results on Example 4.3, which are typical of the
 467 general situation.

468 EXAMPLE 4.4. This is similar to Example 4.2, but the Gaussian has a much

FIG. 4.2. *the evolution of probability given μ and ν in Example 3*

dx	K	N	success	dx	K	N	success
1/16	10	20	✓	1/16	10	20	✓
1/32	10	40	✓	1/32	20	20	✓
1/64	10	80	✓	1/64	20	20	✗
1/128	10	160	✗	1/64	40	20	✓
1/128	10	320	✗	1/128	40	20	✓

TABLE 2
The relationship between dx , K and N in Example 4.3.

469 greater variance. Let $\mathcal{O} = [-0.5, 2.5]$, $dx = 4 \times 10^{-2}$, $K = 80$, $N = 200$, and
470 fix the parameters of initial and terminal Gaussian distributions μ, ν in (4.1) are
471 $a_0 = a_1 = 50$, $b_0 = 0.4$, $b_1 = 1.4$, $r_0 = r_1 = 0.0001$. The evolution of the density is
472 shown in Fig. 4.3, and the sharper behavior of the density evolution with respect to
473 Figure 4.1 is apparent.

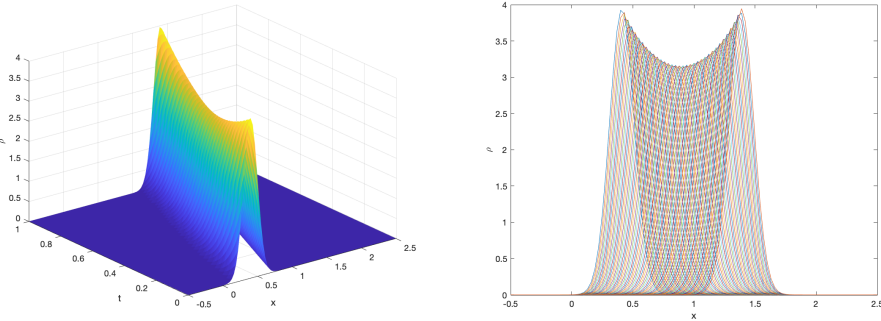
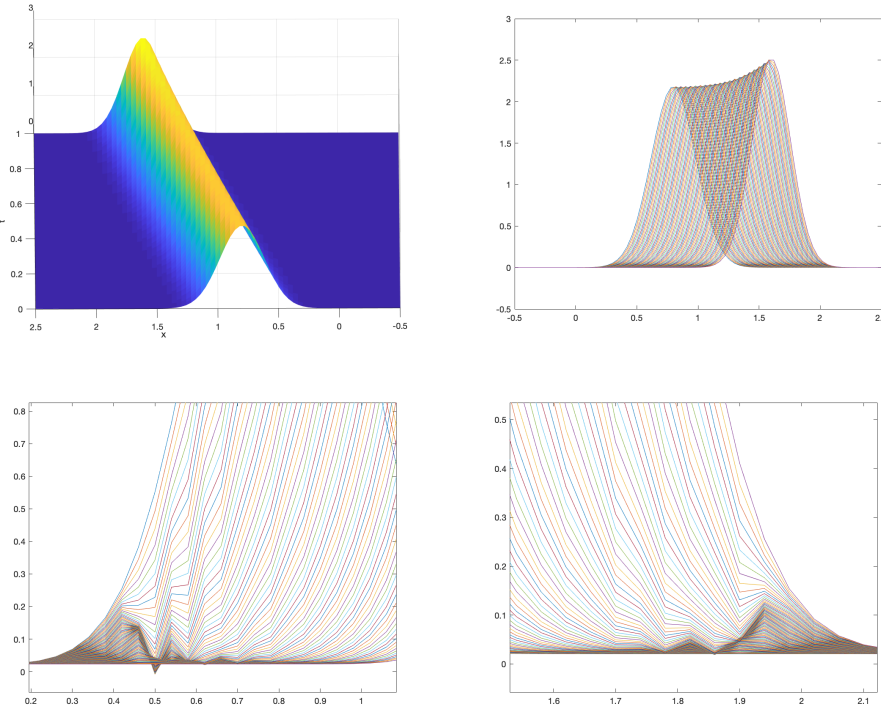
474 EXAMPLE 4.5. This example is used to test Gaussian type distributions μ and ν
475 with different variances. Let $\mathcal{O} = [-0.5, 2.5]$, $dx = 4 \times 10^{-2}$, $K = 80$, $N = 40$, and let
476 the parameters of initial and terminal Gaussian distributions μ, ν are $a_0 = 15$, $a_1 = 10$,
477 $b_0 = 0.8$, $b_1 = 1.6$, $r_0 = r_1 = 0.0001$. The evolution of the density is shown in Figure
478 4.4. In this problem, we also exemplify the impact of the shifting number; as it can be
479 seen in Figure 4.4, if the shifting number is not sufficiently small ($r_0 = r_1 = 0.01$, in
480 this case), one ends up with spurious oscillatory behavior (presently, in $x = [0.4, 0.8]$
481 and $[1.7, 2.1]$).

482 **4.2. 2D numerical experiments.** Here, we give computational results for a
483 computational domain \mathcal{O} which represents a truncation of \mathbb{R}^2 . In Examples 4.6-4.10,
484 we always take $K = 10$ multiple shooting subintervals, $\delta x = 0.2$ as spatial step size,
485 and $N = 30$ integration steps on each subinterval $[t_i, t_{i+1}]$, $t_i = i/K$, $i = 0, \dots, K - 1$.

486 In Examples 4.6-4.7, the initial and/or terminal distributions, μ, ν , are normaliza-
487 tions of Gaussian type densities, namely

$$488 \quad (4.2) \quad \begin{aligned} \hat{\mu} &= \exp(-a_0(x_2 - b_0)^2 - c_0(x_1 - d_0)^2) + r_0, \\ \hat{\nu} &= \exp(-a_1(x_2 - b_1)^2 - c_1(x_1 - d_1)^2) + r_1. \end{aligned}$$

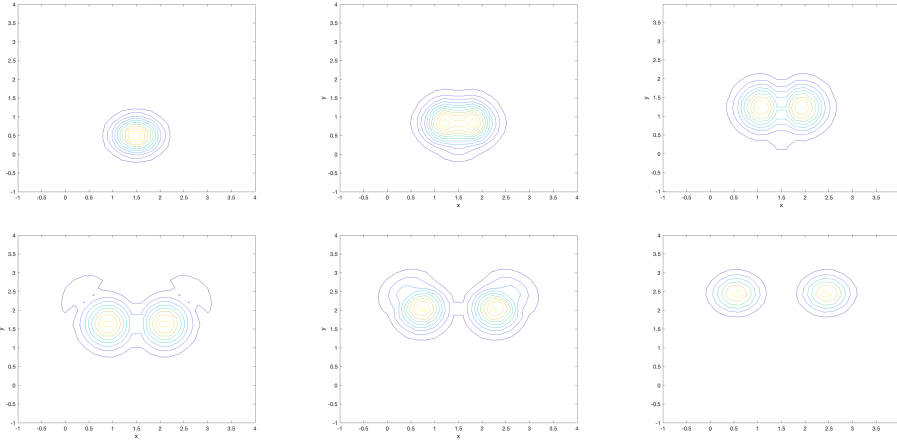
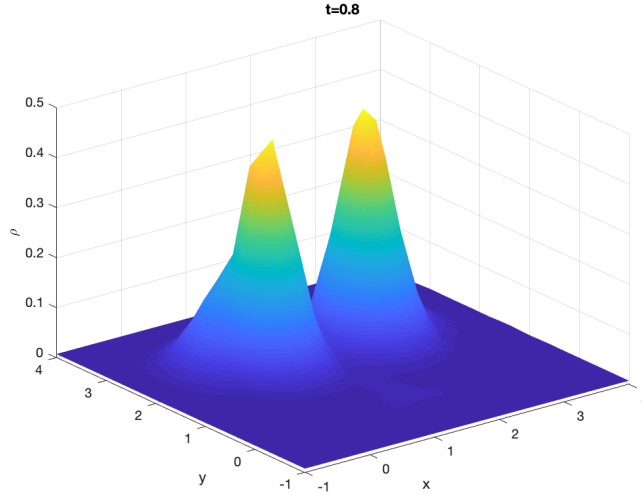
489 EXAMPLE 4.6. Spatial domain is $\mathcal{O} = [-1, 4] \times [-1, 4]$. Initial density is the
490 normalization of the Gaussian type density $\hat{\mu}$ in (4.2), with parameters $a_0 = 5, b_0 =$

FIG. 4.3. *Evolution of probability density in Example 4.4*FIG. 4.4. *Evolution of probability density in Example 4.5 with $r = 0.0001$ (up) oscillator behaviors of probability density when $r = 0.01$ (down)*

491 $0.5, c_0 = 5, d_0 = 1.5, r_0 = 0.01$. The terminal distribution is the normalization of $\hat{\nu}$
 492 below (a two-bump Gaussian)

$$493 \quad \hat{\nu} = \exp(-5(x_2 - 2.45)^2 - 5(x_1 - 2.45)^2) \\ 494 \quad + \exp(-5(x_2 - 2.45)^2 - 5(x_1 - 0.55)^2) + 0.01.$$

496 In Fig. 4.5, we show the contour plots of the density at different times, from which
 497 the formation of the two bumps is apparent. The surfaces of the density at $t = 0.8$
 498 and the two components of initial velocity are shown in Fig. 4.6 and 4.7, respectively.

FIG. 4.5. Example 4.6: contour plots of ρ at $t = 0, 0.2, 0.4, 0.6, 0.8, 1$.FIG. 4.6. Example 4.6: the surface ρ at $t = 0.8$.

499 EXAMPLE 4.7. Spatial domain is $\mathcal{O} = [-1, 3] \times [-1, 3]$. Initial and terminal den-
500 501 502 503 504 505 506 507 508 509 510 511 512 513 514 515 516 517 518 519 520 521 522 523 524 525 526 527 528 529 530 531 532 533 534 535 536 537 538 539 540 541 542 543 544 545 546 547 548 549 550 551 552 553 554 555 556 557 558 559 560 561 562 563 564 565 566 567 568 569 570 571 572 573 574 575 576 577 578 579 580 581 582 583 584 585 586 587 588 589 590 591 592 593 594 595 596 597 598 599 600 601 602 603 604 605 606 607 608 609 610 611 612 613 614 615 616 617 618 619 620 621 622 623 624 625 626 627 628 629 630 631 632 633 634 635 636 637 638 639 640 641 642 643 644 645 646 647 648 649 650 651 652 653 654 655 656 657 658 659 660 661 662 663 664 665 666 667 668 669 670 671 672 673 674 675 676 677 678 679 680 681 682 683 684 685 686 687 688 689 690 691 692 693 694 695 696 697 698 699 700 701 702 703 704 705 706 707 708 709 710 711 712 713 714 715 716 717 718 719 720 721 722 723 724 725 726 727 728 729 730 731 732 733 734 735 736 737 738 739 740 741 742 743 744 745 746 747 748 749 750 751 752 753 754 755 756 757 758 759 750 751 752 753 754 755 756 757 758 759 760 761 762 763 764 765 766 767 768 769 770 771 772 773 774 775 776 777 778 779 770 771 772 773 774 775 776 777 778 779 780 781 782 783 784 785 786 787 788 789 780 781 782 783 784 785 786 787 788 789 790 791 792 793 794 795 796 797 798 799 790 791 792 793 794 795 796 797 798 799 800 801 802 803 804 805 806 807 808 809 800 801 802 803 804 805 806 807 808 809 810 811 812 813 814 815 816 817 818 819 810 811 812 813 814 815 816 817 818 819 820 821 822 823 824 825 826 827 828 829 820 821 822 823 824 825 826 827 828 829 830 831 832 833 834 835 836 837 838 839 830 831 832 833 834 835 836 837 838 839 840 841 842 843 844 845 846 847 848 849 840 841 842 843 844 845 846 847 848 849 850 851 852 853 854 855 856 857 858 859 850 851 852 853 854 855 856 857 858 859 860 861 862 863 864 865 866 867 868 869 860 861 862 863 864 865 866 867 868 869 870 871 872 873 874 875 876 877 878 879 870 871 872 873 874 875 876 877 878 879 880 881 882 883 884 885 886 887 888 889 880 881 882 883 884 885 886 887 888 889 890 891 892 893 894 895 896 897 898 899 890 891 892 893 894 895 896 897 898 899 900 901 902 903 904 905 906 907 908 909 900 901 902 903 904 905 906 907 908 909 910 911 912 913 914 915 916 917 918 919 910 911 912 913 914 915 916 917 918 919 920 921 922 923 924 925 926 927 928 929 920 921 922 923 924 925 926 927 928 929 930 931 932 933 934 935 936 937 938 939 930 931 932 933 934 935 936 937 938 939 940 941 942 943 944 945 946 947 948 949 940 941 942 943 944 945 946 947 948 949 950 951 952 953 954 955 956 957 958 959 950 951 952 953 954 955 956 957 958 959 960 961 962 963 964 965 966 967 968 969 960 961 962 963 964 965 966 967 968 969 970 971 972 973 974 975 976 977 978 979 970 971 972 973 974 975 976 977 978 979 980 981 982 983 984 985 986 987 988 989 980 981 982 983 984 985 986 987 988 989 990 991 992 993 994 995 996 997 998 999 990 991 992 993 994 995 996 997 998 999 1000

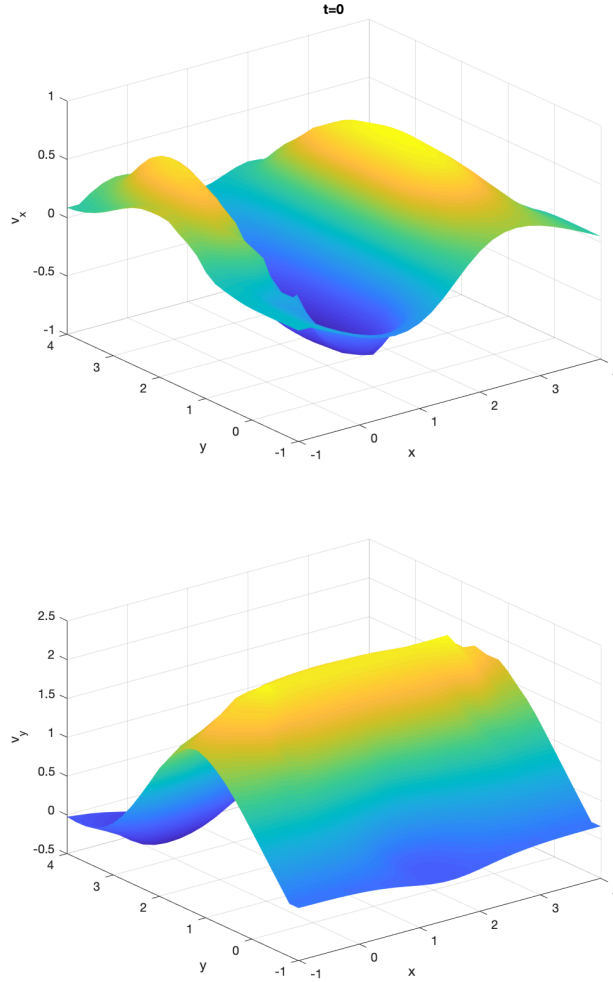


FIG. 4.7. Example 4.6: the two components of the initial velocity.

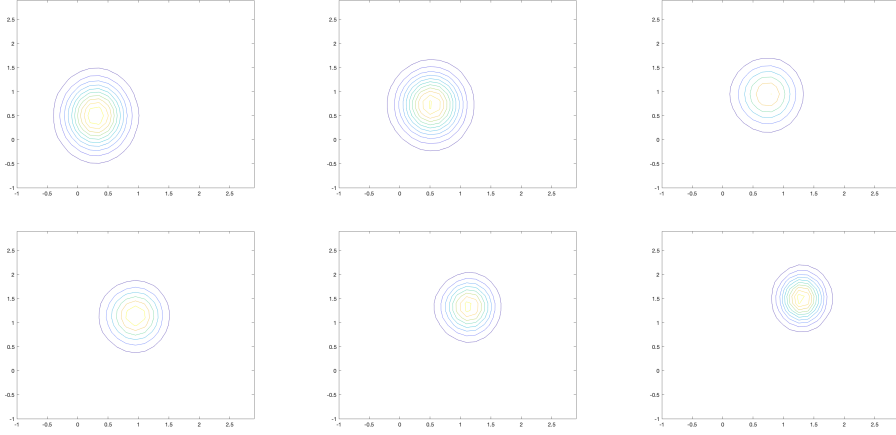
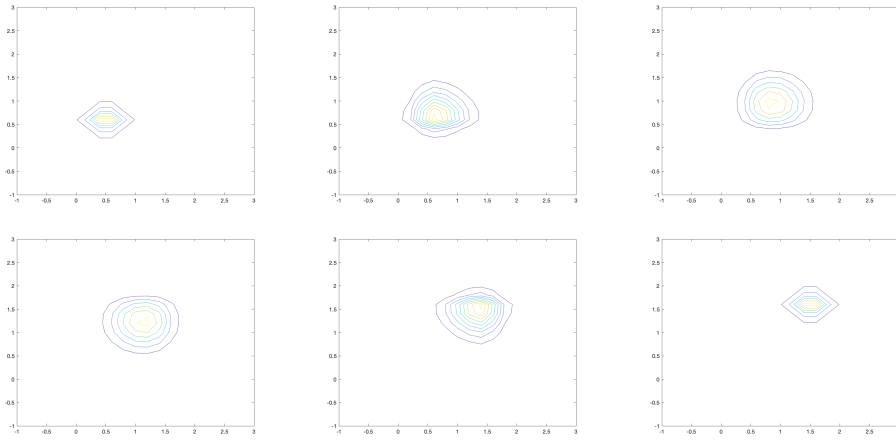
507 EXAMPLE 4.8. Spatial domain $\mathcal{O} = [-1, 3] \times [-1, 3]$. Initial and terminal densities
 508 are normalizations of the Laplace distributions in (4.3) with parameters $a_0 = a_1 =$
 509 $5, b_0 = 0.5, b_1 = 1.5, c_0 = c_1 = 5, d_0 = 0.6, d_1 = 1.6, r_0 = r_1 = 0.001$. Contour plots of
 510 the density evolution are in Fig. 4.9.

511 EXAMPLE 4.9. Spatial domain $\mathcal{O} = [-1, 3] \times [-1, 3]$. Initial density is the uniform
 512 distribution. Terminal density is the normalization of the Laplace distribution $\hat{\nu}$ with
 513 parameters $a_1 = 10, b_1 = 1.5, c_1 = 10, d = 1.6, r = 0.01$. The contour plots of the
 514 density evolution are presented in Fig. 4.10.

515 EXAMPLE 4.10. Spatial domain $\mathcal{O} = [-1, 3] \times [-1, 3]$. Initial density is the nor-
 516 malization of

$$517 \mu = (x_1 + 1)^2(x_1 - 3)^2 + (x_2 + 1)^2(x_2 - 3)^2.$$

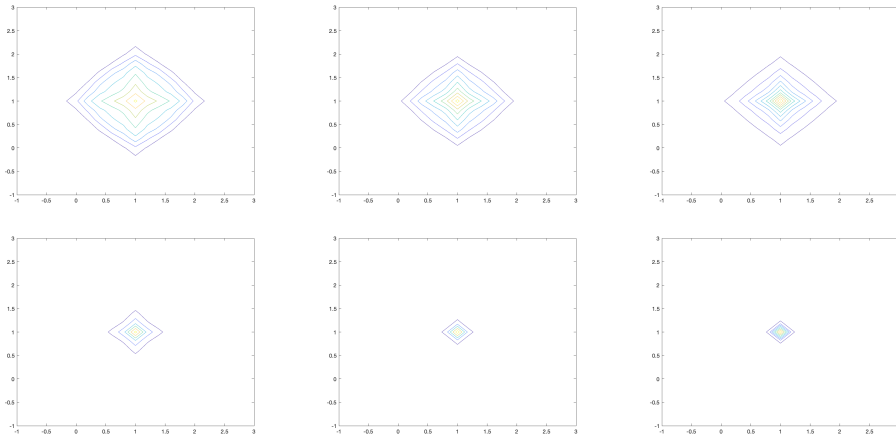
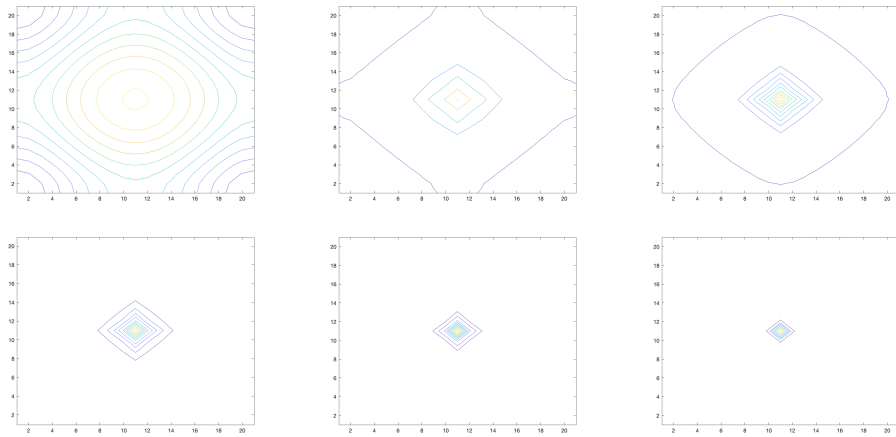
518 Terminal distribution is the normalization of $\hat{\nu}$ in (4.3) with parameters $a_1 = 10, b_1 =$

FIG. 4.8. *Example 4.7: contour plots of ρ at $t = 0, 0.2, 0.4, 0.6, 0.8, 1$.*FIG. 4.9. *Example 4.8: contour plots of ρ at times $t = 0, 0.2, 0.4, 0.6, 0.8, 1$.*

520 $1.5, c_1 = 10, d_1 = 1.6, r_1 = 0.01$. The contour plots of the density evolution are pre-
 521 sented in Fig. 4.11.

522 EXAMPLE 4.11. *Spatial domain $\mathcal{O} = [x_L, x_R] \times [x_L, x_R]$, $x_L = -1, x_R = 3$. The
 523 initial density and terminal distributions are normalized Gaussian densities with pa-
 524 rameters $a_0 = a_1 = 50, b_0 = 0.5, b_1 = 1.5, c_0 = c_1 = 50, d_0 = 0.3, d_1 = 1.3, r_1 = r_2 =$
 525 0.001 . The contour plot of the density evolution is presented in Fig. 4.12.*

526 **5. Conclusions.** In this paper, we proposed a new algorithm for the geodesic
 527 equation with L^2 -Wasserstein metric on probability set. Our algorithm is based on
 528 the Benamou-Brenier fluid-mechanics formulation of the OT problem. Namely, we
 529 view the geodesic equation as a boundary value problem with prescribed initial and
 530 terminal probability densities. To solve the boundary value problem, we adopted the
 531 multiple shooting method and used Newton's method to solve the resulting nonlinear
 532 system. We further adopted a continuation strategy in order to enhance our ability

FIG. 4.10. *Example 4.9: contour plots of ρ at times $t = 0.1, 0.3, 0.5, 0.7, 0.9, 1$.*FIG. 4.11. *Example 4.10: contour plots of ρ at times $t = 0, 0.2, 0.4, 0.6, 0.8, 1$.*

533 to provide good initial guesses for Newton's method. Finally, we presented several
 534 numerical experiments on challenging problems, to display the effectiveness of our
 535 algorithm.

536 There are many interesting questions that remain to be tackled. Surely adaptive
 537 techniques in space and time would be very desirable, especially if one wants to extend
 538 our numerical method to the Wasserstein geodesic equations in higher dimension.
 539 The concern of truncating the spatial domain to a finite computational domain has
 540 not been addressed in our work either, but this is clearly a problem of paramount
 541 importance and will require a careful theoretical estimation of decay rates of the
 542 densities involved. We expect to tackle some of these issues in future work.

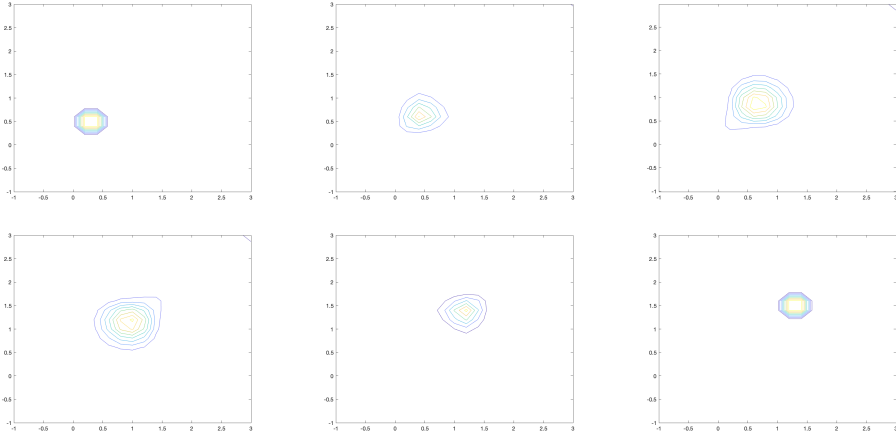


FIG. 4.12. *Example 4.11: contour plots of ρ at times $t = 0, 0.2, 0.4, 0.6, 0.8, 1$.*

544 [1] U. M. Ascher, R. M. Mattheij, and R. D. Russell. *Numerical solution of boundary value*
545 *problems for ordinary differential equations*. Prentice Hall Series in Computational Mathematics. Prentice Hall, Inc., Englewood Cliffs, NJ, 1988.

546 [2] J. D. Benamou and Y. Brenier. A numerical method for the optimal time-continuous mass
547 transport problem and related problems. In *Monge Ampère equation: applications to*
548 *geometry and optimization (Deerfield Beach, FL, 1997)*, volume 226 of *Contemp. Math.*,
549 pages 1–11. Amer. Math. Soc., Providence, RI, 1999.

550 [3] J. D. Benamou and Y. Brenier. A computational fluid mechanics solution to the Monge-
551 Kantorovich mass transfer problem. *Numer. Math.*, 84(3):375–393, 2000.

552 [4] J. D. Benamou, B. D. Froese, and A. M. Oberman. Numerical solution of the optimal trans-
553 portation problem using the Monge-Ampère equation. *J. Comput. Phys.*, 260:107–126,
554 2014.

555 [5] L. A. Caffarelli. Boundary regularity of maps with convex potentials. *Comm. Pure Appl. Math.*,
556 45(9):1141–1151, 1992.

557 [6] Y. Chen, E. Haber, K. Yamamoto, T. T. Georgiou, and A. Tannenbaum. An efficient algorithm
558 for matrix-valued and vector-valued optimal mass transport. *J. Sci. Comput.*, 77(1):79–
559 100, 2018.

560 [7] S. Chow, L. Dieci, W. Li, and H. Zhou. Entropy dissipation semi-discretization schemes for
561 Fokker-Planck equations. *J. Dynam. Differential Equations*, 31(2):765–792, 2019.

562 [8] S. Chow, W. Li, and H. Zhou. Wasserstein Hamiltonian flows. *J. Differential Equations*,
563 268(3):1205–1219, 2020.

564 [9] J. Cui, L. Dieci, and H. Zhou. Time discretizations of Wasserstein-Hamiltonian flows.

565 [10] M. Cuturi. Sinkhorn distances: Lightspeed computation of optimal transport. In C. J. C.
566 Burges, L. Bottou, M. Welling, Z. Ghahramani, and K. Q. Weinberger, editors, *Advances*
567 *in Neural Information Processing Systems*, volume 26. Curran Associates, Inc., 2013.

568 [11] L. Dieci and J. D. Walsh, III. The boundary method for semi-discrete optimal transport
569 partitions and Wasserstein distance computation. *J. Comput. Appl. Math.*, 353:318–344,
570 2019.

571 [12] B. D. Froese. A numerical method for the elliptic Monge-Ampère equation with transport
572 boundary conditions. *SIAM J. Sci. Comput.*, 34(3):A1432–A1459, 2012.

573 [13] W. Gangbo and R. J. McCann. The geometry of optimal transportation. *Acta Math.*,
574 177(2):113–161, 1996.

575 [14] D. Givoli. *Numerical methods for problems in infinite domains*, volume 33 of *Studies in Applied*
576 *Mechanics*. Elsevier Scientific Publishing Co., Amsterdam, 1992.

577 [15] X. Gu, F. Luo, J. Sun, and S. Yau. Variational principles for Minkowski type problems, discrete
578 optimal transport, and discrete Monge-Ampere equations. *Asian J. Math.*, 20(2):383–398,
579 2016.

580 [16] L. V. Kantorovich. On a problem of Monge. *Zap. Nauchn. Sem. S.-Peterburg. Otdel. Mat.*
581 *Inst. Steklov. (POMI)*, 312(Teor. Predst. Din. Sist. Komb. i Algoritm. Metody. 11):15–16,

583 2004.

584 [17] H. B. Keller. *Numerical solution of two point boundary value problems*. Society for Industrial
585 and Applied Mathematics, Philadelphia, Pa., 1976. Regional Conference Series in Applied
586 Mathematics, No. 24.

587 [18] W. Li, P. Yin, and S. Osher. Computations of optimal transport distance with Fisher informa-
588 tion regularization. *J. Sci. Comput.*, 75(3):1581–1595, 2018.

589 [19] L. Métivier, R. Brossie, Q. Mérigot, E. Oudet, and J. Virieux. Measuring the misfit between
590 seismograms using an optimal transport distance: application to full waveform inversion.
591 *J. Funct. Anal.*, 205(1):345–377, 2016.

592 [20] A. M. Oberman and Y. Ruan. An efficient linear programming method for Optimal Trans-
593 portation. *arXiv e-prints*, page arXiv:1509.03668, September 2015.

594 [21] V. I. Oliker and L. D. Prussner. On the numerical solution of the equation
595 $(\partial^2 z / \partial x^2)(\partial^2 z / \partial y^2) - ((\partial^2 z / \partial x \partial y))^2 = f$ and its discretizations. I. *Numer. Math.*,
596 54(3):271–293, 1988.

597 [22] N. Papadakis, G. Peyré, and E. Oudet. Optimal transport with proximal splitting. *SIAM J.*
598 *Imaging Sci.*, 7(1):212–238, 2014.

599 [23] C. R. Prins, R. Beltman, J. H. M. ten Thije Boonkkamp, W. L. Ijzerman, and T. W. Tukker.
600 A least-squares method for optimal transport using the Monge-Ampère equation. *SIAM*
601 *J. Sci. Comput.*, 37(6):B937–B961, 2015.

602 [24] E. K. Ryu, Y. Chen, W. Li, and S. Osher. Vector and matrix optimal mass transport: theory,
603 algorithm, and applications. *SIAM J. Sci. Comput.*, 40(5):A3675–A3698, 2018.

604 [25] F. Santambrogio. *Optimal transport for applied mathematicians*, volume 87 of *Progress in Non-*
605 *linear Differential Equations and their Applications*. Birkhäuser/Springer, Cham, 2015.
606 Calculus of variations, PDEs, and modeling.

607 [26] E. Tenetov, G. Wolansky, and R. Kimmel. Fast entropic regularized optimal transport using
608 semidiscrete cost approximation. *SIAM J. Sci. Comput.*, 40(5):A3400–A3422, 2018.

609 [27] C. Villani. *Optimal transport*, volume 338 of *Grundlehren der Mathematischen Wissenschaften*
610 [*Fundamental Principles of Mathematical Sciences*]. Springer-Verlag, Berlin, 2009. Old
611 and new.

612 [28] H. Weller, P. Browne, C. Budd, and M. Cullen. Mesh adaptation on the sphere using optimal
613 transport and the numerical solution of a Monge-Ampère type equation. *J. Comput. Phys.*,
614 308:102–123, 2016.